A Throughput Drop Estimation Model and Its Application to Joint Optimization of Transmission Power, Frequency Channel, and Channel Bonding in IEEE 802.11n WLAN for Large-Scale IoT Environments

ARTICLE INFO

Keywords:
Internet of Things
WLAN
partially overlapping channel
access point
transmission power
channel bonding
non-channel bonding
throughput drop

ABSTRACT

The concept of *Internet of Things (IoT)* has been widely studied in smart home networks, smart city networks, smart grid systems, autonomous driving systems, and smart healthcare systems. In IoT, the IEEE 802.11n *wireless local-area network (WLAN)* is used as a common communication technology due to its flexibility and low cost. Then, the high performance WLAN is required to enhance *quality of service (QoS)* of large-scale IoT applications connecting a number of devices or sensors allocated in wide areas. WLAN can use the limited number of *partially overlapping channels (POCs)* at *2.4 GHz* band. The WLAN performance can be degraded by interfered signals from other WLANs. Then, to optimize the POC assignment by reducing interferences, we have proposed the *throughput drop estimation model* for concurrently communicating multiple links under interferences. Unfortunately, the *40 MHz channel bonding (CB)* and the *20 MHz non-CB* are considered separately, while the transmission power is always fixed to the maximum. In this paper, we study the *throughput drop estimation model* under coexistence of *CB* and *non-CB* while the transmission power is changed. Then, we present its application to the joint optimization of assigning the transmission power, the frequency channel, and the channel bonding to enhance the throughput performance of IEEE 802.11n WLAN. For evaluations, we compare estimated throughputs by the model with measured ones in various network topologies to verify the model accuracy. Then, we apply the model to the joint assignment optimization in them, and confirm the effectiveness through simulations and experiments using the testbed system.

1. Introduction

Nowadays, the concept of *Internet of Things (IoT)* has become popular world-wide. IoT has been used to provide various communication services, like smart home networks and smart city networks among others [1, 2, 3, 4]. IoT adopts wireless communication and networking technologies to support communications between devices [5].

For IoT applications, the *wireless local-area network (WLAN)* and the *wireless sensor network (WSN)* play important roles [6]. Basically, a lot of IoT applications adopt client-server type of communications using the *IEEE 802.11 WLAN*, as in Figure 1 [4, 6]. A large number of IoT devices are connected to the Internet through WLANs. These WLANs are densely deployed using many *access points (APs)*. However, dense APs often interfere with each other, and can severely degrade the communication performance. Therefore, the performance enhancement of WLAN under interferences is strongly needed.

The WLAN performance under interferences can be enhanced by properly assigning the transmission power, the frequency channel, and the channel bonding (CB) to each AP. In conventional WLAN, computer hosts communicate with servers in the Internet, while IoT devices communicate with servers. Therefore, in this paper, a *host* is sometimes used to represent a *IoT device*.

The *IEEE 802.11 WLAN* has been deployed world-wide to support the Internet access due to its flexibility, low cost, and high data transmission [7]. It can operate in two unlicensed frequency bands of *2.4 GHz* and *5 GHz*. The *2.4 GHz* is generally adopted because of the wide coverage range with the stronger penetration capability in indoor environments [8].

ORCID(S):

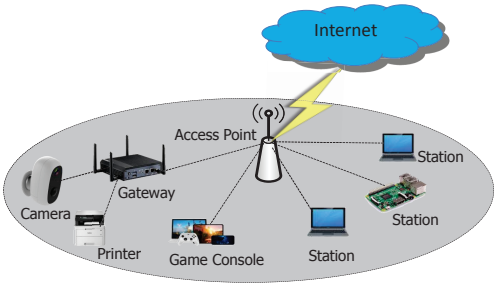

Figure 1: WLAN for IoT application.

The IEEE 802.11 standard defines the limited number of frequency channels for communications. At *2.4 GHz*, the spectrum of adjacent channels is partially overlapped with each other, called the *partially overlapping channels (POCs)*. The IEEE 802.11n and the later standards support *channel bonding (CB)* by combining two neighbouring *20 MHz* channels together to form one *40 MHz* channel to increase the transmission capacity. Figures 2 (a) and (b) illustrate the *2.4 GHz* spectrum with *20 MHz non-CB* and *40 MHz CB* respectively, to demonstrate the POCs in IEEE 802.11n.

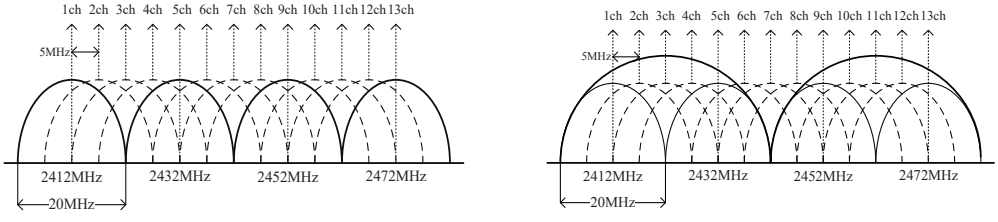

(a) 20 MHz POCs at 2.4 GHz band. (b) 40 MHz POCs at 2.4 GHz band.

Figure 2: 2.4 GHz non-bonding channels and bonding.

In [9], *CB* increases the number of sub-carriers for data transmissions with Orthogonal Frequency Division Multiplexing (OFDM) to 108 from 52 in the conventional non-CB channel. In this wide-band CB, the OFDM uses multiple narrow-band carriers to transfer data for the higher throughput.

The CB can increase the number of frames to be transmitted together by the frame aggregation, because of the higher bit-rate with the increased number of data sub-carriers to send data frames as a bundle. With the fixed pulse length for packet transmissions, the CB can send more data bits than the non-CB. The frame aggregation can reduce the overhead induced by the CSMA/CA protocol to send multiple frames in a single bundle and be acknowledged together over a single channel access

However, the CB reduces the number of non-interfered channels and can cause more interferences in dense WLANs. In [10], the wider bandwidth of the CB link can cause the reduction of *signal to interference plus noise ratio (SINR)* at the distant host from the AP. The lower *SINR* can cause the adoption of the slower *modulation and coding scheme (MCS)* and the *hidden terminal problem*, thus lower throughput. It has been observed that the simultaneous use of CB and non-CB can improve the WLAN performance [11].

In WLAN, the maximum transmission power of the AP can maximize the transmission capacity and range but can also maximize the interference to other APs. However, when a host is located near to the AP, the minimum transmission power can provide the same maximum throughput due to the non-linear relationship between the *received signal strength (RSS)* and throughput and can reduce the interference. Thus, it has been observed that either the maximum or minimum transmission power of each AP can offer the highest overall throughput of the WLAN.

To support a large number of IoT devices and hosts allocated in a wide area and provide seamless Internet connections, WLANs are often deployed densely using a lot of APs. Since the number of available channels is limited, each WLAN may face multiple interferences from co-located other WLANs. Thus, to enhance the overall throughput performance, it is a key challenge to jointly optimize the transmission power, the

frequency channel, and the CB assignment to each AP in the WLAN, considering the *throughput drop* by the interferences from other WLANs.

Previously, we studied the *throughput drop estimation model* for multiple interfered links using either CB only [12] and non-CB only [13]. The model estimates the *throughput drop* of the target link that is caused by the interfered links, considering the *channel distance (chD)* and the *interfered received signal strength (RSS^i)* at the target AP from the interfered AP. The *chD* of the two links is defined as the minimum channel difference between the channels of the links, while the RSS^i refers to the interfered received signal strength at the AP of the target link from the AP of the interfered link. To obtain the nominal throughput of the target link under multiple interfered links, the throughput under no interference is first estimated using the model in [14]. Then, it is subtracted by the *throughput drop* estimated for each of the interfered links sequentially, in descending order of the throughput drop magnitude.

In this paper, first, we study the *throughput drop estimation model* for concurrently communicating links under coexistence of *CB* and *non-CB* with different transmission powers. This model exploits the advantages of *CB* and *non-CB* together and can be used to optimize the transmission power to increase the throughput under interferences. The parameters of this model are newly adjusted based on measurement results under coexistence of *CB* and *non-CB* links with various conditions of channel distances. Then, we apply this model to the joint optimization of assigning the transmission power, the frequency channel, and the channel bonding in IEEE 802.11n WLAN.

For evaluations, we compare estimated throughputs by the model with measured ones in various network topologies, and verify the model accuracy. Then, we apply the model to the joint assignment optimization in them, and confirm the effectiveness through simulations and experiments using the testbed system.

The rest of this paper is organized as follows: Section 2 presents related works in literature. Section 3 reviews our previous works related to this paper. Section 4 presents throughput drop measurements under coexistence of *CB* and *non-CB* links. Section 5 presents the proposed model and its evaluations. Section 6 presents the application to the joint optimization and its evaluations. Finally, Section 7 concludes this paper with future works.

2. Related Works

A significant amount of research works has addressed the problem of interferences in WLANs to enhance the throughput performance by the proper channel assignment [15, 16] and the transmission power control.

In [16], Mishra et al. showed that the *orthogonal channel (OC)* assignment to APs in WLAN can be inefficient in a network field, if a substantial number of APs are co-located there. In [17], Mishra et al. demonstrated that the careful design of the POC allocation to APs in WLAN can improve the performance with the efficient spatial reuse.

In [18], Zhao et al. showed that the effects of interferences on the performance depend on the channel separation and the degree of the frequency overlapping among the interfered links. In particular, the simultaneous interferences from two links will cause the higher deterioration of the performance than the single interference, which is smaller than the summation of the individual ones.

In [19, 20], Zhao et al. and Mukherjee et al. considered the sum of the interfering signal powers at the target node, when more than one APs are interfering. Since the MAC protocol lowers the data transmission rate of the target AP, depending on the level of the individual interference, the simple summation of the individual interferences may fail to identify the real value for the interference. Based on this suggestion, our paper examines individual interferences sequentially from the largest to the smallest.

In [21], Vanhatupa et al. presented the *graph coloring approach (GCA)* to acquire a solution for the channel assignment. A feasible solution only occurs when available channels can provide a *colored graph*. When a *colored graph* is not possible, this GCA has no qualitative ordering of possible solutions.

In [22], Nabil et. al. presented a mathematical approach to optimally use *CB* to meet the stochastic user demands. In their work, the number of bonded channels can be increased or decreased depending on the throughput demand of each AP. However, it does not present a model to estimate the throughput demands of APs. It is assumed that one *non-CB* channel can satisfy one unit of the AP demand.

In [23], Tewari et al. proposed a joint approach for the power tuning and the POC assignment. In their proposal, the APs in the network field are activated one by one, and transmission power is initially

set to maximum. Then, POCs under conventional *20 MHz non-CB* are assigned, and transmission power is reduced considering neighbor interfered APs while ensuring that each AP serves the largest number of hosts and satisfies the minimum host throughput threshold. They also proposed the AP placement through the power control and the POC assignment in [24]. Here, the similar approach in [23] is adopted, where the appropriate location of every AP is also considered to reduce interference while maximizing the number of hosts served. Their works adopt the conventional *non-CB* channels and is evaluated only through simulation. On the other hand, we observed that simultaneous use of CB and non-CB can give better performance, thus adopted in our proposal. Additionally, we optimize the assignment of these POCs jointly with transmission power and evaluated through simulation and test bed experiments.

In [25], Kachroo et. al. proposed a joint channel assignment and transmission power control algorithm for a multi-rate WLAN where the conventional 20 MHz *non-CB* POC channels are used. Initially, the algorithm assigns the channels to the APs while keeping the transmission power constant. Then, it optimizes the transmission power such that the *signal to interference plus noise ratio (SINR)* is maximized and the coverage area threshold is maintained for every AP. Their proposal was evaluated only through simulation. On the other hand, our proposal adopts joint optimization of CB and non-CB POCs, and transmission power to maximize the total network throughput.

In [26], Raval et. al. demonstrated the importance of the efficient hardware and high throughput network to support the IoT. They showed that adopted devices consume a significant amount of energy. Therefore, they proposed the energy management system for IoT devices to optimize the energy consumption.

3. Review of Previous Works

In this section, we review our previous works related to this paper.

3.1. Definitions of Three Distances

First, the *channel distance*, the *physical distance*, and the *link distance* are defined to describe the throughput drop estimation model under POCs.

(a) *Channel distance (chD)* represents the minimum channel difference between the channels of the two links. For example, when both links are assigned the same channel, *chD* is 0, where they will be fully overlapped. On the other hand, when one link is assigned *channel 1* and another link *channel 3*, *chD* is 2.

(b) *Physical distance (phD)* represents the Euclidean distance between the two APs of the links. By increasing the *phD* between the links, the interfered signal fades due to the path loss and the absorption by obstacles.

(c) *Link distance (lkD)* represents the Euclidean distance between the transmitter and receiver of the link. Since the signal is propagated from the transmitter to the receiver, the longer *lkD* reduces the RSS at the receiver and can degrade the throughput.

3.2. Throughput Estimation Model under Non-Interference

In [14], we presented the *throughput estimation model* for a single link under no interference. This model estimates the *receiving signal strength (RSS)* at the host using the *log distance path loss model* [27]:

First, the Euclidean distance *d (m)* is calculated for each link (AP/host pair) by:

$$d = \sqrt{(AP_x - H_x)^2 + (AP_y - H_y)^2} \tag{1}$$

where AP_x, AP_y and H_x, H_y does the x and y coordinates for the AP and the host respectively.

Then, *d (m)* is used to estimate RSS_d in Eq. (2) by:

$$RSS_d = P_1 - 10\alpha \log_{10} d - \sum_k n_k W_k \tag{2}$$

where RSS_d represents RSS $(-dBm)$ at the host, P_1 does RSS at $1m$ distance from the AP when no obstacle exists, α does the path loss exponent, *d(m)* does the Euclidean distance between the AP and the host, n_k does the number of *type_k* obstacles along the path from the AP to the host, and W_k does the signal attenuation factor (dBm) for *type_k* obstacle. The parameters P_1, α, and W_k are obtained by running our parameter optimization tool [28] with the measurement data.

Next, this model converts RSS_d to the estimated throughput tp_{ij} using the *sigmoid function*:

$$tp_{ij} = \frac{a}{1 + e^{-(\frac{(120+RSS_d)-b}{c})}} \tag{3}$$

where tp_{ij} represents the estimated throughput $(Mbps)$ and a, b, and c are constant coefficients whose values were obtained by running our parameter optimization tool [28] with the measurement data.

3.3. Throughput Drop Model for Interfered Link under CB

In [12, 29], we presented the *throughput drop estimation model* under interfered CB links. For two interfered links, this model adopts the *logarithm function* of the RSS, RSS^i and the chD from the interfered link in Eq. (4).

$$tpD(RSS^i, chD) = p(chD) \times \ln(q(chD) + RSS^i) + r(chD) \tag{4}$$

where $tpD(RSS^i, chD)$ indicates the estimated throughput drop $(Mbps)$, and $p(chD)$, $q(chD)$, and $r(chD)$ represent the constants determined by the channel distance (chD). The *physical distance* (phD) between the two APs is closely related with the RSS (RSS^i) of the interfered signal at the AP. When phD increases, the corresponding RSS^i decreases, as shown in Eq. (2) where RSS_d represents RSS^i and d does phD. The values of the three constant parameters in Eq. (4), p, q, and r, in Table 1 are computed from the throughput drop measurement results for each chD by running *Origin Pro8* software [30]. The devices and software in Table 4 were used in measurements.

When two or more interfered links exist, we observed that the throughput drop becomes higher than that of a single link interfere, but less than the simple sum of the individual throughput drops by all the interfered links [13, 18, 31]. Thus, in the model, the interfered links are explored sequentially in descending order of their drops. The interfered link causing the highest drop is considered first. For this largest interfered link, the target link adopts the more robust modulation and coding scheme and reduces the throughput. Then, the interfered link causing the second highest drop is considered, which further reduces the throughput by increasing the contention. The following procedure is applied;

1. Estimate the throughput of the target link using the model under non-interference.
2. Estimate the throughput drop *tpD* from each interfered link using Eq. (4).
3. Sort the links in descending order of the drop magnitude. Here, the two interfered links are considered to the target link, where the drops are given by tpD^{1st} and tpD^{2nd}.
4. For the largest interfered link, adjust tpD^{1st} by the maximum speed of the AP of the target link, because the different APs may have the different throughput performances. The largest interfered link is defined as the interfered link that causes the largest throughput drop (*tpD*) at the target link.

$$tpD^{1st}_{adj} = tpD^{1st} \times \frac{tpM^{AP}}{140} \tag{5}$$

where tpD^{1st}_{adj} represents the adjusted throughput drop by the largest interfered link, tpM^{AP} does the maximum throughput for the AP of the target link, and 140 does the maximum throughput (Mbps) under channel bonding (CB) for NEC AP adopted in the model.

Then, the throughput tp_{ij}^{1st} of the target link is estimated after considering the drop by the first interfered link by:

$$tp_{ij}^{1st} = tp_{ij} - tpD_{adj}^{1st}. \tag{6}$$

5. For the second interfered link, adjust the tpD^{2nd} by:

$$tpD_{adj}^{2nd} = tpD^{2nd} \times \frac{tpM^{AP} - tpD_{adj}^{1st}}{140}. \tag{7}$$

The throughput tp_{ij}^{2nd} of target link is estimated after considering the drop by the second interfered link by:

$$tp_{ij}^{2nd} = tp_{ij}^{1st} - tpD_{adj}^{2nd}. \tag{8}$$

6. If more interfered links exist, repeat the same procedure.

The actual value of the throughput drop depends on the throughput range of the device at the target link. Eq. (4) was introduced to estimate the throughput drop, where the maximum link-speed of the target link is 140 Mbps for *NEC WG2600HP* AP device with CB used in the experiments. For other device whose maximum speed is different from 140 Mbps, this value needs to be adjusted linearly by its maximum speed as confirmed in our experiments.

3.4. Throughput Drop Model for Interfered Link under non-CB

In [13], we presented the *throughput drop estimation model* under interfered *non-CB* links. From our measurement results, the *natural logarithm function* in Eq. (4) is again used to estimate the *throughput drop* (tpD) for *non-CB* links. The parameter values are newly tuned from measurement results of each chD as in Table 2.

For three or more interfered links, the interfered links are explored sequentially in descending order of their throughput drops as for CB links. First, the throughput drop in Eq. (5) and Eq. (7) is adjusted to consider the difference of the maximum throughput of the APs for *non-CB* ($75Mbps$) and CB ($140Mbps$) as follows:

$$tpD_{adj}^{1st} = tpD^{1st} \times \frac{tpM^{AP}}{75} \tag{9}$$

$$tpD_{adj}^{2nd} = tpD^{2nd} \times \frac{tpM^{AP} - tpD_{adj}^{1st}}{75} \tag{10}$$

Then, the dropped throughput under the interferences for the target link is obtained by sequentially subtracting the tpD_{adj}^{1st} and tpD_{adj}^{2nd} from tp_{ij}, as in Eq. (6) and Eq. (8).

3.5. Rate Adaptation Algorithm and Significance of Model Approach

In this subsection, we discuss the rate adaptation algorithm and the significance of our throughput estimation model approach.

Table 1
Throughput drop estimation model parameters for CB.

channel distance	p	q	r
0	27	88.17	-20
1	27	87.36	-20
2	27	89.00	-22
3	25	94.50	-22
4	33	92.00	-56
5	34	92.00	-57
6	45	91.00	-98
7	45	88.00	-100
8	40	75.50	-80

Table 2
Throughput drop estimation model parameters for non-CB.

channel distance	p	q	r
0	16.0	90.0	-14
1	17.0	74.5	-14
2	16.0	75.0	-14
3	16.0	73.0	-14
4	13.0	72.0	-13
5	5.5	73.0	-8

3.5.1. Rate Adaptation Algorithm

The *IEEE 802.11 standard* defines the rate adaptation algorithm with the *modulation and coding scheme (MCS)* indexes for the *medium access control (MAC)* protocol. For each MCS index, the maximum supported data rate is defined. Although the specific implementation details can differ by Wi-Fi card vendors, the rate adaptation algorithm defined in the standard is basically same.

In [32], the dynamic rate adaptation is used to choose the best data rate that allows the establishment of communications. Different Wi-Fi card vendors may apply different parameters to control the rate dynamically, such as the signal level, the rate of data packet retries, and the channel conditions. The most popular logic in the dynamic rate adaptation is the *auto rate fall-back mechanism* [33, 34], where the data rate is reduced based on the current link performance. Therefore, the performance of the proposed model is not affected by the specific implementation of the rate adaptation algorithm by different Wi-Fi card vendors.

3.5.2. Significance of Model Approach

The TCP/IP uses several functions at packet communications such as the *three-way handshaking* mechanism for establishing a connection by the transmission request and the acknowledgment (ACK) reception, and the *TCP window control* to dynamically control the amount of data segments the sender can send and be received successfully by the receiver. Initially, the TCP connection will start with a small window size (less data segments) and every time there is a successful ACK, the window size will increase (more data segments). When the sender does not receive ACK for some data segments, it re-transmits them and the window size will be reduced [35].

Besides, in wireless networks, the *back-off window control* mechanism is adopted to resolve contentions among different stations wishing to transmit data at the same time. The *fragmentation burst* and the *frame aggregation* are adopted to transmit multiple packets continuously or bundled. Therefore, it becomes difficult to estimate the throughput from the accurate values of all the parameters of the protocol stack, including the MCS index, the TCP window size, and the frame aggregation.

Instead, we define and use the empirical approximate equations to estimate the RSS, the throughput, and the throughput drop. These equation are derived from extensive experiments using various devices/ Wi-Fi network interface cards [13, 14, 36]. The *log-distance path loss model* [27] is for the received signal strength (RSS), the *sigmoid function* is for the throughput from RSS, and the *log function* is for the throughput drop

from the interfered received signal strength (RSS^i).

4. Throughput Drop Measurements under Coexistence of CB and non-CB Links

In this section, we present throughput drop measurements under coexistence of *CB* and *non-CB* links.

4.1. Measurement Setup

Figure 3 illustrates the measurement setup for two links. The hardware and software in Table 4 are adopted in measurements. These devices are set up on the *third floor of Engineering Building #2* at Okayama University in Figure 6 (a).

For the throughput measurements, *Iperf 2.0.5 software* [37] is adopted as a popular tool for measuring the TCP throughput by generating TCP packets. This software automatically saturates the TCP traffics at a link. Then, for each measurement point in Figure 4 and other related figures, the TCP traffic was generated with *477KB TCP window size and 8KB buffer size* for *four minutes* at intervals of *30 seconds*, which was conducted twice on different days. Then, the average value is computed for each point and is presented in the figures. The packet size of the TCP traffic generated is *1,500 bytes*. To eliminate the fluctuations in measurements, the average of the measured throughput during *four minutes* at intervals of *30 seconds* on two different days is computed for each point.

The RSS of both *Link1* and *Link2* in Figure 3 is measured by executing the *"iwconfig wlan0 | grep Link"* Linux command at *AP1* for *Link1* and *AP2* for *Link2* for *two minutes* at *one second* intervals. Then, the average measured RSS for both links is used to represent the RSS^i (-dBm) in Figure 5. By increasing the *phD* between *Link1* and *Link2* from $5m$ to larger, the different RSS^i was measured.

For each point of the measured RSS^i, the throughputs were also measured for both links. Then, the *throughput drop* was given by the difference between the average throughput for the single link and the concurrently communicating links. This procedure was repeated by assigning several channels at the APs for the two links so that they had different channel distances as demonstrated in Figure 5.

To fixed the channel in *NEC WG2600HP* AP adopted in our experiments, one of the 13 channels for the 20MHz width is selected as the primary channel through the *graphical user interface (GUI)*. To increase the channel width to 40MHz by the channel bonding, the GUI provides the corresponding option to set the primary channel to the channel bonding. Then, the 20MHz primary channel is bonded with the adjacent 20MHz secondary channel to form the 40MHz channel. Table 3 summarizes how channel bonding is achieved.

Table 3
Bonded channels.

20MHz		40MHz
primary channel	secondary channel	bonded channel
1	5	1+5
2	6	2+6
3	7	3+7
4	8	4+8
5	9	5+9
6	10	6+10
7	11	7+11
8	12	8+12
9	13	9+13

In this measurements, the channel of the first link is fixed at *CB channel 1+5*, and that of the second link is changed from *non-CB channel 1* to *non-CB channel 13*.

4.2. Measurement Results

First, we examine the throughput measurement results under interferences between two adjacent links. From the results of the individual links under interferences, it is discovered that the individual throughput always fluctuates, since the contentions among the links are not well resolved by the *carrier sense mechanism*

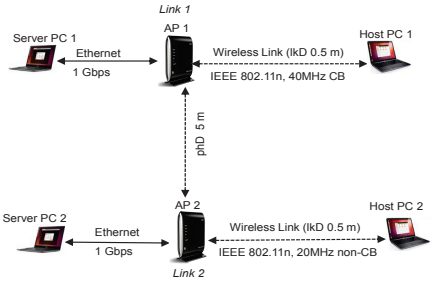

Figure 3: Measurement setup.

Table 4
Devices and Software for Measurements.

access point ($all\ links$)	
model	NEC WG2600HP
operating mode	IEEE 802.11n
operating band	2.4 GHz
channel width	40 MHz or 20 MHz
wireless NIC	Atheros XSPAN [38]
host PC ($all\ links$)	
model	Toshiba dynabook R731/B
OS	Ubuntu 14.04 LTS (kernel 3.13.0-57)
processor	Intel Core i5-2520M 2.54 Ghz
chipset	Intel HM65 Express
wireless NIC	Atheros AR938x [39]
server PC ($link_1$)	
model	Toshiba dynabook R731/B
OS	Ubuntu 14.04 LTS (kernel 3.13.0-57)
processor	Intel Core i5-2520M 2.54 Ghz
chipset	Intel HM65 Express
wireless NIC	Atheros AR938x
server PC ($link_2$, $link_3$)	
model	Fujitsu lifebook S761/C
OS	Ubuntu 14.04 LTS (kernel 4.2.0-27)
processor	Intel Core i5-2520M 2.5GHz
chipset	Mobile Intel QM67 Express
wireless NIC	Atheros XSPAN [40]

[41]. It can cause the unfair channel occupancy among them. Besides, the throughput performance of one link on CB is different from that of $non\text{-}CB$. Thus, we will use the sum of the throughputs from the two links in our evaluations.

Figure 4 shows the total throughput of the two links under no interference case, one wall case between APs *(phD = two rooms)*, and $phD = 5m$ case at different chD. In the experiments, the link distance (lkD) between a host and an AP is fixed at $0.5m$.

For $chD = 4$ or smaller channel distances, the total throughput for the two links is similar, because the $non\text{-}CB$ interference level from the CB link is not changed regardless of the channel distance. By shifting $non\text{-}CB$ from channel 1 to 5, it is still fully overlapped with CB on *1+5*.

Then, from $chD = 5$ to $chD = 7$, the throughput slightly decreases due to increasing interferences from non-target APs in the environment, where most of them use $non\text{-}CB$ channel 6. For $chD = 8$ or larger channel distances, the throughput increases due to less interferences. It becomes maximum at $chD = 12$ where no interference exists.

Figure 5 shows the changes of the total throughput drop of the two links for a different chD. Here, $lkD = 0.5m$ is fixed, and phD is changed from $3m$ to larger ones to obtain the different RSS^i. The total throughput

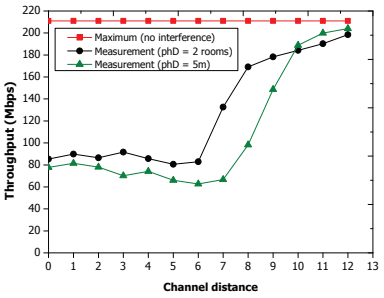

Figure 4: Total throughput of two links coexisting under CB and non-CB for different chD and phD.

drop for the small chD and strong RSS^i is large while that of the large chD and weak RSS^i is small for less interference.

5. Throughput Drop Estimation Model under Coexistence of CB and non-CB Links

In this section, we present the *throughput drop estimation model* under coexistence of *CB* and *non-CB* links by extending previous works.

5.1. Throughput Drop Estimation Model for Two Interfered Links

From throughput drop measurement results in Figure 5, the *natural logarithm function* can again be used to estimate the *throughput drop (tpD)* from the interfered *received signal strength* (RSS^i) and the *channel distance (chD)*, as in Eq. (4). The parameters for the throughput drop estimation model are newly tuned under coexistence of *CB* and *non-CB* as in Table 5 by running *Origin Pro8* software.

Table 5
Throughput drop estimation model parameters for coexistence of CB and non-CB.

channel distance	p	q	r
0	40.5	85.0	-10.0
1	40.0	83.0	-10.0
2	41.5	81.0	-9.0
3	41.0	78.5	-7.0
4	40.0	81.0	-8.0
5	42.0	79.0	-7.0
6	41.0	81.0	-7.0
7	39.0	80.0	-7.0
8	35.0	80.0	-7.0
9	26.0	75.0	-9.0
10	20.0	75.0	-8.0
11	14.0	80.0	-8.0
12	9.0	81.0	-8.0

For evaluations of this model, the center frequency is used as the channel number of CB. For $1 + 5$ CB channel, the channel becomes 3. The parameters in Table 5 are obtained by shifting *non-CB* from channel 1 to channel 13. Hence, the largest is $chD = 12$.

The non-CB has channel 1 to channel 13, while CB has channel 3 to channel 11. Therefore, for the CB channel 3, $chD = 2$ appears when non-CB channel is 1 or 5, where it is the minimum channel distance between the channels of the two links. Similarly, $chD = 1$ appears when non-CB channel is 2 or 4. In Figure 4, for $chD = 4$ or smaller channel distances, the total throughput for the two links is almost same since the channel of *non-CB* link fully overlaps with the *CB* link in Figure 2 (b). Similarly, the parameter values for $chD = 4$ or smaller channel distances are similar. Therefore, when the non-CB channel is 5 or smaller,

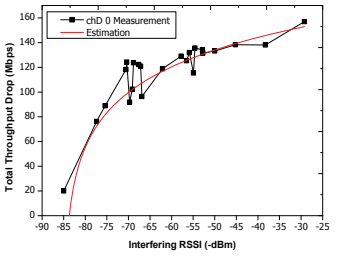

(a) $chD = 0$

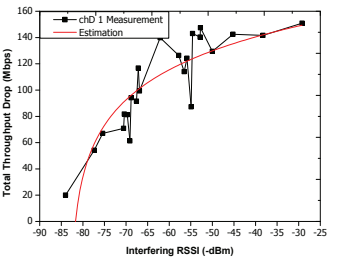

(b) $chD = 1$

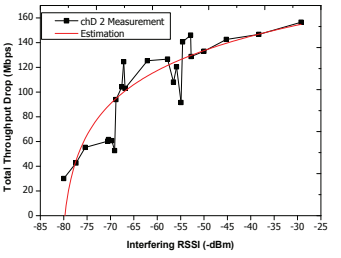

(c) $chD = 2$

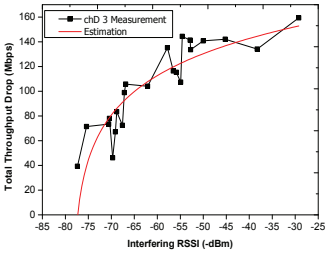

(d) $chD = 3$

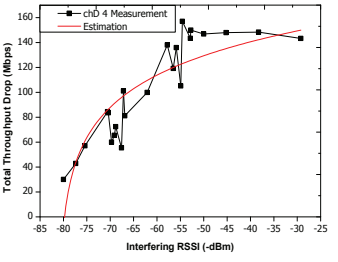

(e) $chD = 4$

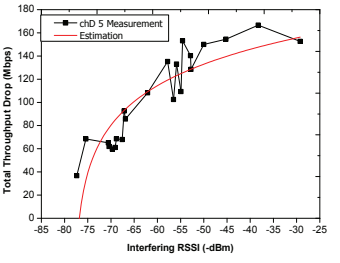

(f) $chD = 5$

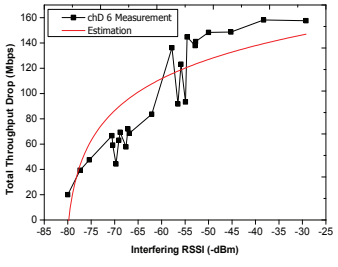

(g) $chD = 6$

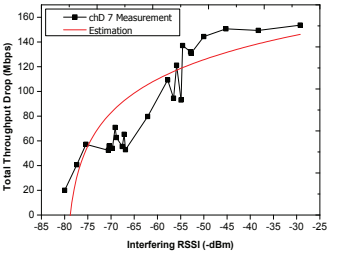

(h) $chD = 7$

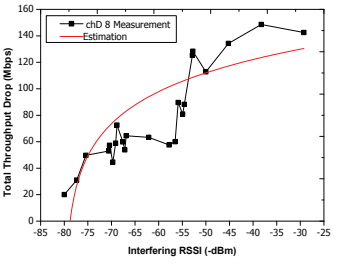

(i) $chD = 8$

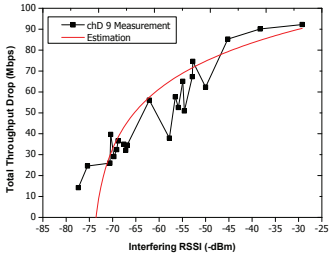

(j) $chD = 9$

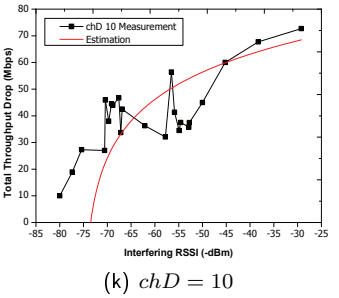

(k) $chD = 10$

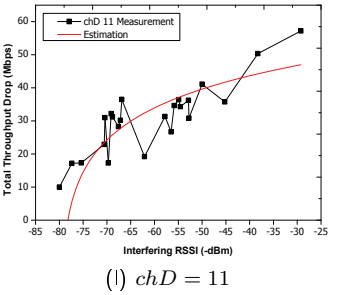

(l) $chD = 11$

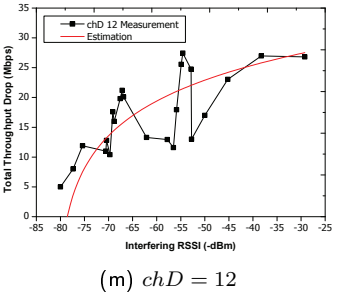

(m) $chD = 12$

Figure 5: Total throughput drop results for different interfered RSS at different chD.

the throughput drop is estimated by taking the estimated average by parameters for $chD = 0$ to $chD = 4$. When the non-CB channel is 6 or larger, the estimation is done using parameters for $chD = 5$ or larger.

5.2. Throughput Drop Estimation Model for Multiple Interfered Links

Then, the throughput drop estimation model for multiple interfered links is considered. Again, the interfered links are explored sequentially in descending order of their throughput drops. It is noted that only two interfered links are described here.

1. When both of the interfering APs adopt *CB*, estimate the throughput drop under *CB* in [29].
2. When both of the interfering APs adopt *non-CB*, estimate the throughput drop under *non-CB* in [13].
3. When one AP adopts *CB* and another does *non-CB*, the following procedure is applied:
   (a) Estimate the single link throughput for each host by Eq. (2) and Eq. (3).
   (b) Estimate the sum of the throughput drops for the two APs by Eq. (4) using the parameters in Table 5.
   (c) Sort the links in descending order of the throughput drops that are given by tpD^{1st} and tpD^{2nd}.
   (d) For the largest interfered link, adjust tpD^{1st} with the maximum speed of the target AP by Eq. (11) and Eq. (12).

$$tpD^{1st}_{adj} = tpD^{1st} \times \beta \times \frac{tpM^{AP}}{140}. \tag{11}$$

$$tpD^{1st}_{adj} = tpD^{1st} \times \beta \times \frac{tpM^{AP}}{75}. \tag{12}$$

   It is assumed that one AP represents the target AP and the other does interfering AP. Eq. (11) is applied if the target AP uses *CB*, and Eq. (12) is applied otherwise. β represents the throughput drop normalization factor of 0.635 for *CB* and 0.365 for *non-CB*.
   (e) For the second interfered link, adjust the tpD^{2nd} by Eq. (13) and Eq. (14) for the target AP with CB and the AP with *non-CB* respectively.

$$tpD^{2nd}_{adj} = tpD^{2nd} \times \beta \times \frac{tpM^{AP} - tpD^{1st}_{adj}}{140}. \tag{13}$$

$$tpD^{2nd}_{adj} = tpD^{2nd} \times \beta \times \frac{tpM^{AP} - tpD^{1st}_{adj}}{75}. \tag{14}$$

   Then, the dropped throughput under the interferences for the target link is obtained by sequentially subtracting tpD^{1st}_{adj} and tpD^{2nd}_{adj} from tp_{ij}, as in Eq. (6) and Eq. (8).
   (f) If more interfered links exist, repeat the same procedure.

5.3. Application of Transmission Power Optimization to Throughput Drop Estimation Model

As demonstrated in [42], the minimum transmission power at the AP can provide throughput similar to that of maximum transmission power when the host is located near the AP due to the non-linear relationship between *RSS* and the throughput. At the same time, the minimum transmission power can reduce interferences among the co-located APs. When the host is located far from the AP, the maximum transmission

power at the AP is necessary to provide the sufficient RSS for the better throughput. Therefore, in the throughput drop estimation model, the power is tuned to improve the throughput.

In [43], when the transmission power is changed, the P_1 value in Eq. (2) is changed while the other parameter values are fixed. In the proposed model, the same Eq. (2) is applied to estimate both the *received signal strength (RSS)* at the host from the AP and the *interfered received signal strength (RSS^i)* at the target AP from the interfering AP. In [42], either the *maximum* or *minimum* transmission power at the AP was selected since other powers do not cause significant throughput changes. Therefore, the proposed model adopts the P_1 values only for the maximum or minimum transmission power at CB and non-CB in Table 6.

Table 6
P_1 values for each transmission power.

channel	transmission power	P_1
CB	maximum	-20.0
	minimum	-33.2
non-CB	maximum	-28.2
	minimum	-33.2

5.4. Evaluation of Model Estimation Accuracy

The accuracy of the proposed model is evaluated for links by comparing the estimated throughput results with the measured ones, when the AP is assigned either the maximum or minimum transmission power under *CB case*, *non-CB case*, and coexistence case of *CB* and *non-CB*. The same hardware and software in Table 4 are adopted.

5.4.1. Network Fields

The third floor of Engineering Building #2 at Okayama University in Figure 6 (a) is used. In this field, several other WLANs can be observed, which may cause interference to the target link in our experiments. Fortunately, the signals from them are weaker than the signals of our devices. First, we show the evaluation results for two interfered links. Then, we show them for three links.

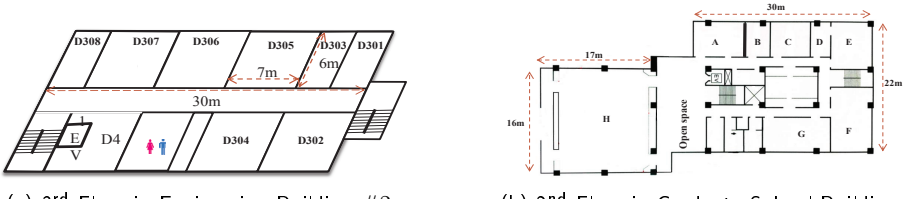

(a) 3rd Floor in Engineering Building #2. (b) 2nd Floor in Graduate School Building.

Figure 6: Network fields.

5.4.2. Results for Two Interfered Links

The two links in Figure 3 are setup in the network field in Figure 6 (a). Figures 7, 8, and 9 illustrate the throughput measurement and estimation results for *CB case*, *non-CB case*, and coexistence case of *CB* and *non-CB* respectively, under different transmission power combinations.

For *CB case* in Figure 7, the channel of the first link is fixed at *CB channel 1+5*, and that of the second link is changed from *CB channel 1+5* to *CB channel 9+13*. In (a), the APs of the two links are assigned the maximum transmission power while in (b), the minimum power is assigned. In (c), one AP is assigned the maximum power while the other AP is the minimum power.

For *non-CB case* in Figure 8, the channel of the first link is fixed at *non-CB channel 1*, and that of the second link is changed from *non-CB channel 1* to *non-CB channel 7* where they do not interfere. Again, in (a), the APs of the two links are assigned the maximum transmission power while in (b), the minimum power is assigned. In (c), one AP is assigned the maximum power while the other AP is the minimum power.

For *coexistence of CB* and *non-CB case* in Figure 9, the channel of the first link is fixed at *CB channel 1+5*, and that of the second link is changed from *non-CB channel 1* to *non-CB channel 13*. The APs for

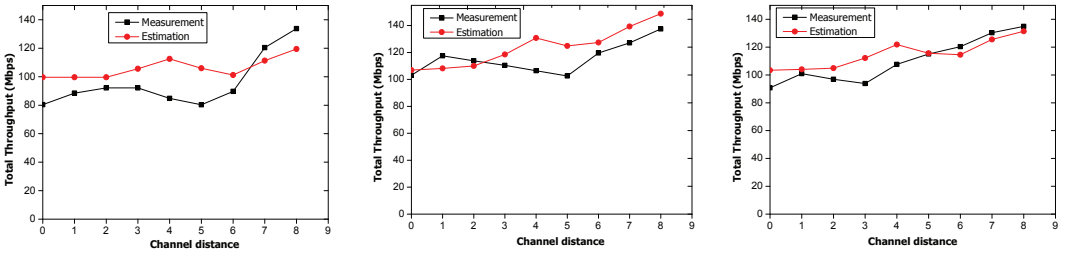

(a) CB links all max. power (b) CB links all min. power (c) CB links max. and min. power

Figure 7: Throughput measurement and estimation results for two links under all CB.

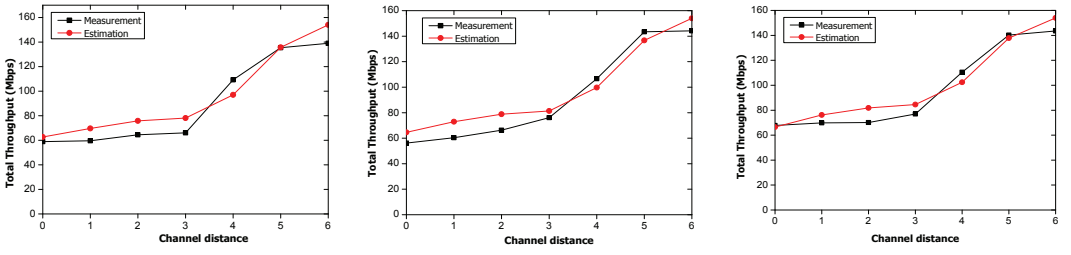

(a) non-CB links with all max. power (b) non-CB links with all min. power (c) non-CB links with max. and min. power

Figure 8: Throughput measurement and estimation results for two links under all non-CB.

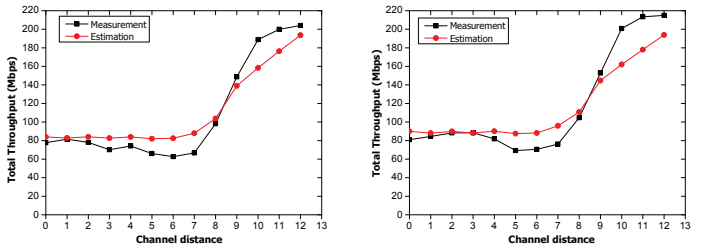

(a) Coexistence of CB and non-CB links with all max. power (b) Coexistence of CB and non-CB links with all min. power

Figure 9: Throughput measurement and estimation results for two links under coexistence of CB and non-CB.

both links are assigned the maximum transmission power in (a) while the minimum power is used in (b).

To demonstrate the throughput estimation accuracy of the proposed model, Table 7 summarizes the average absolute errors (Mbps) obtained by Eq. (15) between the measured throughputs and the estimated ones in *Figures 7, 8,* and *9*. This table indicates that the absolute error is relatively small in any case, which demonstrates the sufficient accuracy of the proposal. It is noted that uncontrollable interferences from other WLANs in the network field can increase the error.

$$AverageAbsoluteError = \frac{1}{n}\sum_{i=1}^{n}|measured_i - estimated_i| \tag{15}$$

where n represents total number of data.

5.4.3. Results for Three Interfered Links

The network field in Figure 6 (a) is adopted. AP_1, AP_2 and AP_3 are located in rooms *D307*, *D306* and *refresh corner* respectively. Figure 10 illustrate the throughput measurement and estimation results for *CB*

Table 7
Average absolute errors of throughput drop estimation model.

channel	transmission power	average absolute error (Mbps)
CB	all max.	15.49
	all min.	11.42
	max/min.	7.87
non-CB	all max.	9.23
	all min.	8.88
	max/min.	6.84
joint CB and non-CB	all max.	13.26
	all min.	14.45

case and coexistence of *CB* and *non-CB case*. The *non-CB case* was not evaluated here since the three links would not interfere.

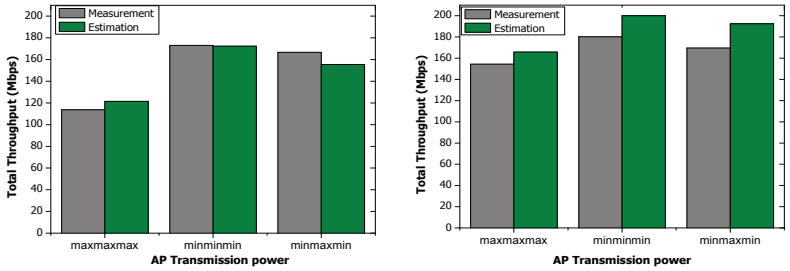

(a) All CB case (b) Coexistence of CB and nonCB case

Figure 10: Throughput measurement and estimation results for three links under only CB and coexistence of CB and non-CB.

For *CB case* in Figure 10 (a), *CB channel 5+9* for AP_1, *CB channel 1+5* for AP_2, and *CB channel 9+13* for AP_3 are assigned. For *coexistence case of CB and non-CB* in Figure 10 (b), *CB channel 9+13* for AP_1, *non-CB channel 13* for AP_2, and *CB channel 1+5* for AP_3 are assigned. Then, for each of the two cases, the measured throughputs are compared with estimated ones when the three APs are assigned the maximum power, minimum power and two APs are assigned the minimum and the other AP is assigned the maximum transmission power.

The comparisons of measured and estimated throughput results confirm the high accuracy of the proposed model under various channel and transmission power conditions among two or three links. However, small gaps between the measured and estimated throughputs can appear due to interferences from non-target WLANs in the network field.

5.5. Evaluation for Different AP Device

To verify the generality of the proposed model, we evaluate the accuracy using different AP devices.

5.5.1. Measurement Scenario

We adopt the *Raspberry Pi 3 Model B* for the AP that is configured by the procedure in [44]. This device uses Raspbian OS, Broadcom BCM2837, 1.2Ghz 64-bit quad-core ARM Cortex-A53 CPU, LPDDR2-900MHz 1GB SDRAM, 10/100Mbps Ethernet, IEEE802.11b/g/n wireless NIC, and Blue-tooth 4.1 classics/low energy [45]. This device does not support *CB*. Thus, we use *TP-Link TL-WN722N USB NIC* adapter for CB [46].

To set the channel width, we can edit the */etc/hostapd/hostapd.conf* file with the following Linux commands:

```
$ #20MHz
$ rsn_pairwise=TKIP
```

```
$#40MHz
$ rsn_pairwise=CCMP
$ ht_capab=[HT40+][SHORT-GI-20][SHORT-GI-40][DSSS_CCK-40][MAX-AMSDU-3839]
```

The *[HT40+]* needs to set the 20MHz primary channel in */etc/hostapd/hostapd.conf* file. Then, the primary channel will be bonded with the secondary channel in Table 3 to form the 40MHz channel.

In [13], it was demonstrated that the *Raspberry Pi 3 Model B* has the similar throughput drop characteristic to the *NEC AP* used in the proposed model. However, the maximum achievable throughput by *Raspberry Pi* AP is smaller, which is *40 Mbps* and *53 Mbps* for *non-CB* and *CB* respectively. Therefore, in the proposed model, the estimated values by the model are normalized using Eq. (16) as follows;

$$tpD_{pi} = tpD_{nec} \times \frac{tpM^{pi}}{tpM^{nec}} \tag{16}$$

where tpD_{nec} represent the throughput drop for *NEC AP*, tpM^{pi} and tpM^{nec} does the maximum throughput for *Raspberry Pi* and *NEC* APs respectively.

5.5.2. Results and Discussions

The network field in Figure 6 (a) is used to evaluate the three interfered links under coexistence of CB and non-CB channels. The channel of each AP is fixed at *non-CB channel 1* for AP_1, *CB channel 9+13* for AP_2, and *CB channel 1+5* for AP_3. Figure 11 shows the measured and estimated throughput results for three scenarios.

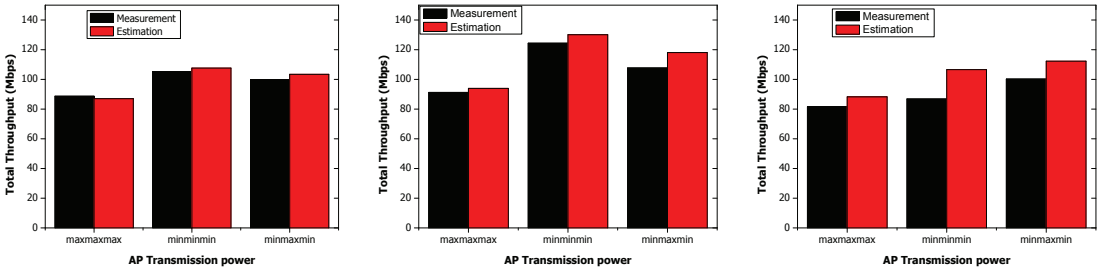

(a) Scenario 1 (b) Scenario 2 (c) Scenario 3

Figure 11: Throughput measurement and estimation results for Raspberry Pi AP.

(1) Scenario 1

AP_1 and AP_2 are located in room *D306* and AP_3 in the corridor in front of *D303*. The link distance of each host is *0.5m*. In this scenario, these APs interfere with each other, and the minimum power offers the higher throughput.

(2) Scenario 2

AP_1 is located in room *D307*, AP_2 in *D306* and AP_3 in the corridor in front of *D303*. The link distance of each host is *0.5m*. In this scenario, the APs have less interferences than in *Scenario 1*. Hence, the minimum power offers the higher throughput.

(3) Scenario 3

The locations of the APs is similar to *Scenario 2*. The link distance of the hosts is *0.5m* except for the host connected to AP_2. It is moved to the corridor in front of *D4*. In this scenario, the minimum power to AP_1 and AP_3 and the maximum power to AP_2 offers the higher total throughput since the host connected to AP_2 is located far from it while other hosts are located near to their APs. Again, the estimated throughput is well matched with the measured ones for the three scenarios. Therefore, the proposed model can be used for various AP devices.

6. Model Application to Joint Optimization Algorithm

In this section, we present the application of the proposed model to the joint optimization of the transmission power, the frequency channel and the channel bonding of the APs in WLAN through the extension of the *active AP configuration algorithm* in [47].

6.1. Modifications of Active AP Configuration Algorithm

The channel assignment phase of the algorithm is modified to assign *CB* and *non-CB POCs* together with the proper transmission power to each AP using the proposed model. Specifically, the modifications of this phase are described as follows.

6.1.1. Input and Output

In the algorithm input, the number of channels C_{CB} for *CB POC*s and C_{non} for *non-CB POC*s, and the center frequency of each channel are given.

In the algorithm output, the *CB* or *non-CB POC* and the *maximum* or *minimum* transmission power is assigned to each active AP, instead of *non-CB orthogonal channels (OC)* with the conventional *maximum* transmission power.

6.1.2. Objective

In the algorithm objective, the new cost function E_{ch} in Eq. (17) is designed to maximize the total throughput of the links in WLAN.

$$E_{ch} = \sum_{i=1}^{N} TP_i^{POC} \tag{17}$$

where TP_i^{POC} represents the total throughput of the links associated with AP_i and N is total number of APs.

TP_i^{POC} is calculated by:

$$TP_i^{poc} = \sum_{j}^{m} \left(tp_{ij}^{poc} \times Srf\left(m\right) \right) \tag{18}$$

where m represents the number of hosts associated with AP_i, tp_{ij}^{POC} does the estimated throughput of the link between AP_i and $host_j$ by the proposed model, and $Srf(m)$ does the contention factor at AP_i for associated hosts to send data through CSMA/CA. $Srf(m)$ is calculated by:

$$Srf\left(m\right) = \left(\frac{1}{m + \frac{0.1(m-1)}{4}} \right) \times 1 - \left(0.1 \times m - 1\right). \tag{19}$$

The constants in Eq. (19) are obtained from our extensive measurements in increasing the number of associated hosts to a single AP one by one under no interference.

6.1.3. Procedure for Joint Optimization

Initially, only *CB* channels with the maximum transmission power are assigned by the greedy procedure, since they can maximize the throughput in general. Then, this assignment is improved by optimizing the selection of *CB*, *non-CB*, the maximum power, and the minimum power by the following steps:

1. Randomly select one AP with the maximum transmission power for the change trial.
2. Randomly select a different CB channel from the current one to this selected AP.

3. Run the throughput estimation model. If the estimated throughput improves E_{ch} in Eq. (17), this channel change is accepted. To avoid the local optimum, the hill-climbing procedure is applied where if 0-1 random number is smaller than exp(DeltaE_{ch}/Temp), where DeltaE_{ch} is difference between old and new E_{ch} and Temp is given algorithm parameter for temperature, this channel change is accepted.
4. Go back to step 1, when the new channel is accepted. Otherwise, go to the next step.
5. Change the transmission power to the minimum and run step 3.
6. Go back to step 1, when the new power is accepted. Otherwise, go to the next step.
7. Change the selected channel to *non-CB* and run step 3.
8. Go back to step 1, when the new non-CB is accepted. Otherwise, go to the next step.
9. Change the transmission power to the maximum and run step 3.
10. Go back to step 1.

6.2. Evaluations

To evaluate the joint optimization algorithm using the model, we conduct simulations using the model and compare the estimated results with test-bed measurement results in several network topologies. In each topology, the performance by the proposal is compared with those by two conventional approaches in literature, *1) CB only*, and *2) non-CB only*. For each of the two conventional approaches, the results for both the *maximum* and *minimum* transmission power are presented.

6.2.1. Network Fields

The third floor of Engineering Building #2 and the second floor of Graduate School of Natural Science and Technology Building at Okayama University in Figure 6 (a) and (b) respectively, are used. Table 8 shows the locations of the APs and the hosts in the fields for each topology.

Table 8
Device Locations

network field	topology	device locations		
		AP1, Host1	AP2, Host2	AP3, Host3
Eng.Bldg. #2	1	D306	D306	D306
	2	D307	D307	D307, D306
	3	D306	D306	corr. near D303
	4	D308	corr. near D301	refresh corner
Grad. Sch.Bldg.	1	H	H	H
	2	open space	A	B

6.2.2. Results for Engineering Building

Figures 12 to 15 show the total throughput results by measurements and simulations. Each figure compares the total throughput by the proposal with the ones by *CB only* and *non-CB only* with the maximum and minimum transmission powers as conventional approaches.

In Figure 12 and 13, the three APs are located in the same room and are interfered with each other. To reduce the interference, the proposal assigns the three *non-CB channel* 1, 7, and 13, and the minimum transmission power to the APs in Figure 12. In Figure 13, AP_1 and AP_2 are assigned the minimum power because they are located in the same room, while AP_3 is assigned the maximum power because the associated host is in the different room.

In Figure 14, AP_1 and AP_2 are located in the same room and AP_3 is located far from them. Due to less interferences, the proposal assigns *joint non-CB channel* 13, and *CB channel* $1+5$ and $9+13$ to AP_1, AP_2, and AP_3 respectively. The minimum transmission power is assigned to all the APs because they are located in the same room as the associated hosts.

In Figure 15, the three APs are located far from each other. Thus, there is few interference between them. The proposal assigns *CB channel* $1+5$, $9+13$, and $5+9$ to AP_1, AP_2, and AP_3 respectively. The transmission power becomes minimum because they are located in the same room as the associated hosts.

The simulation results by the model and the measurement results are similar to each other. The performance results by the proposal are better than those by the comparison methods, or at least similar where the proposal assigns the same channel and transmission power as the comparison methods. These results demonstrate the effectiveness of the proposal.

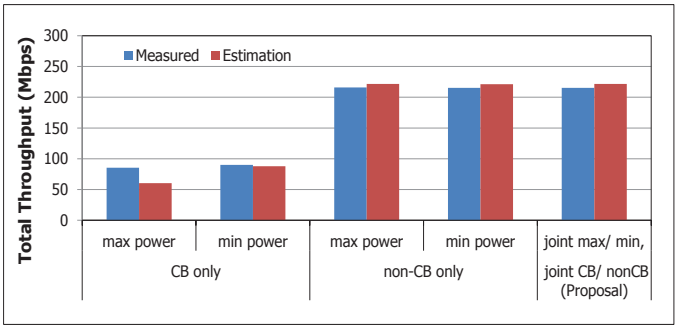

Figure 12: Results for topology 1 in Engineering Building.

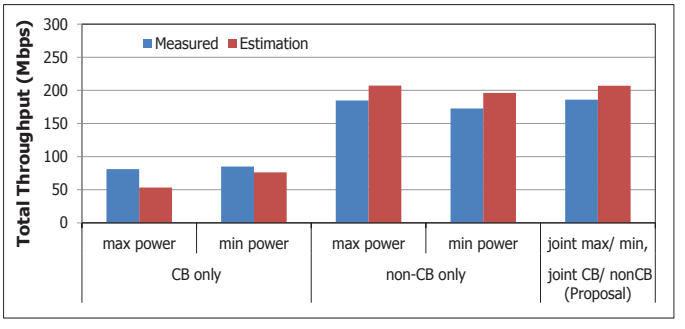

Figure 13: Results for topology 2 in Engineering Building.

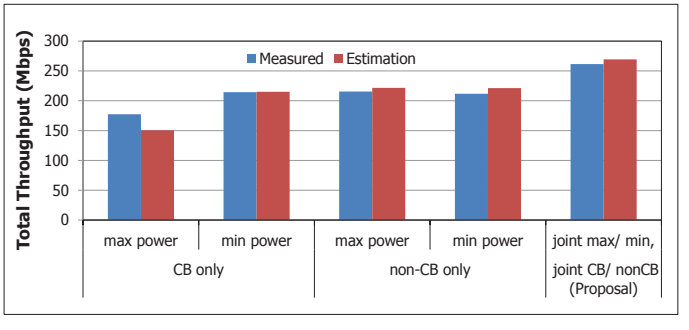

Figure 14: Results for topology 3 in Engineering Building.

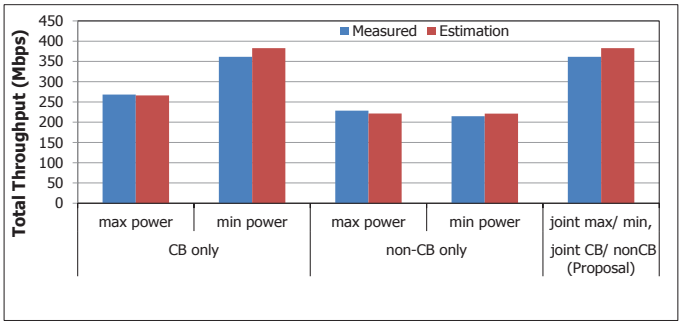

Figure 15: Results for topology 4 in Engineering Building.

6.2.3. Results for Graduate School Building

Figure 16 and 17 show the total throughput results for measurements and simulations by the model. In Figure 16, the three APs are located in the same room. To reduce interferences, the proposal assigns *non-CB channel* 1, 7, and 13 and the minimum transmission power to AP_1, AP_2, and AP_3 respectively.

In Figure 17, the three APs are located relatively far from each other. Due to less interferences, the proposal assigns *CB channel* $9+13$, $1+5$, and *non-CB channel* 13 and the minimum transmission power to AP_1, AP_2, and AP_3 respectively. The proposal gives the better performance than the comparison methods.

The simulation results by the model and the measurement results are similar to each other in them. The performance results by the proposal are better or at least similar to the comparison methods. These results confirm the effectiveness of the proposal in different network fields.

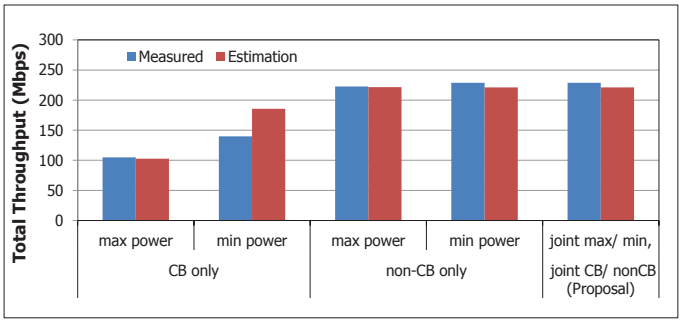

Figure 16: Results for topology 1 in Graduate School Building.

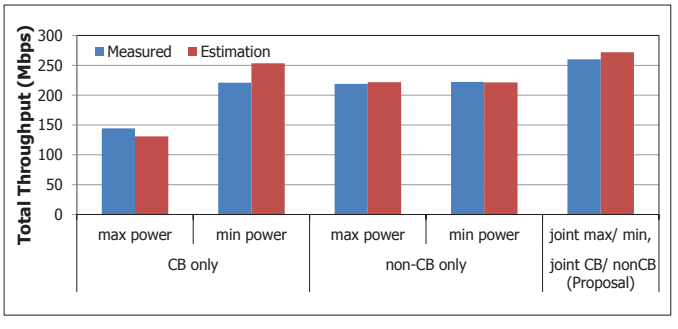

Figure 17: Results for topology 2 in Graduate School Building.

Table 9 summarizes the average absolute errors (Mbps) between the measured throughputs and the

estimated ones for the joint optimization application in *Figures 12 to 17*. The table indicates that the absolute error is relatively small in any case except for the two cases where interferences from other WLANs in the network field increased the error.

Table 9
Average absolute errors for model application to joint optimization.

channel	transmission power	average absolute error (Mbps)	
		Eng. Bldg. #2	Grad. Sch. Bldg.
CB	max.	20.76	7.76
	min.	8.29	39.17
non-CB	max.	10.38	1.86
	min.	11.31	4.16
proposal (joint optimization)	optimized	14.25	9.63

6.2.4. Standard Deviation

In this subsection, we show the standard deviation of the proposed approach in Tables 10 and 11. As demonstrated in both tables, the value of standard deviation is small. Although there are several factors that can affect the performance of wireless local area networks such as interference from non-target APs in the network field, the standard deviation of the proposed approach is still small. Again, this demonstrates the robustness of the proposal.

Table 10
Average standard deviation of model evaluations in figures 7 and 8

channel distance	0	1	2	3	4	5	6	7	8
Avg. SD	5.774	6.173	6.454	7.633	11.01	6.806	7.144	6.130	6.887

Table 11
Average standard deviation of model application to joint optimizations in figures 12 to 17

channel	transmission power	Avg. SD
CB	max	11.49
	min	13.14
non-CB	max	5.335
	min	6.314
Proposal (joint optimization)	optimized	8.985

7. Conclusion

This paper presented the *throughput drop estimation model* for concurrently communicating multiple links under coexistence of *channel bonding* and *non-bonding* with different transmission powers in IEEE 802.11n WLAN, and its application to the joint optimization of the transmission power, the frequency channel, and the channel bonding of the APs considering large-scale IoT environments. The accuracy of the proposed model was confirmed by comparing the estimated throughputs with the measured ones under various network topologies. The effectiveness of the joint optimization using the model was verified through simulations by the model and experiments. In future works, we will further improve the model to better its accuracy and evaluate it through extensive simulations and experiments.

References

[1] S. Zeadally and O. Bello, Harnessing the power of Internet of Things based connectivity to improve healthcare, Internet of Things, pp. 100074, 2019.

[2] H.A. El Zouka and M.M. Hosni, Secure IoT communications for smart healthcare monitoring system, Internet of Things, pp. 100036, 2019.
[3] D. Mocrii, Y. Chen, P. Musilek, IoT-based smart homes: A review of system architecture, software, communications, privacy and security, Internet of Things, vol. 1, pp. 81-98, 2018.
[4] M. M. Islam, N. Funabiki, R. W. Sudibyo, K. I. Munene, and W. C. Kao, A dynamic access-point transmission power minimization method using PI feedback control in elastic WLAN system for IoT applications, Internet of Things, vol. 8, pp. 100089, 2019.
[5] J. O. Agyemang, J. J. Kponyo, G. S. Klogo, J. O. Boateng, Lightweight rogue access point detection algorithm for WiFi-enabled Internet of Things (IoT) devices, Internet of Things, vol. 11, pp. 100200, 2020.
[6] H. Hanseul, Y. Y. Kim, and R. Y. Kim, A low-power WLAN communication scheme for IoT WLAN devices using wake-up receivers, Appl. Sci., vol. 8, no. 1, pp. 1-16, 2018.
[7] B. P. Crow, I. Widjaja, J. G. Kim, and P. T. Sakai, IEEE 802.11 wireless local-area networks, IEEE Commun. Mag., vol. 35, no. 9, pp. 116-126, Sept. 1997.
[8] J. Talvitie, M. Renfors, and E. S Lohan, A comparison of received signal strength statistics between 2.4 GHz and 5 GHz bands for WLAN-based indoor positioning, in Proc. Globecom Work., pp. 1-6, 2015.
[9] National Instrument, Introduction to wireless LAN measurements from 802.11a to 802.11ac., 2018.
[10] S. Barrachina-Muñoz, F. Wilhelmi, and B. Bellalta, To overlap or not to overlap: enabling channel bonding in high-density WLANs, Comp. Netw., vol. 152, pp. 40-53, 2019.
[11] K. I. Munene, N. Funabiki, H. Briantoro, M. M. Rahman, S. C. Roy, and M. Kuribayashi, A study of throughput drop estimation model for concurrently communicating links under coexistence of channel bonding and non-bonding in IEEE 802.11n WLAN, in Proc. Int. Work. Virt. Env. Netw.-Ori. Appl., pp. 700-714, July, 2021.
[12] K. I. Munene, N. Funabiki, M. M. Islam, M. Kuribayashi, M. S. A. Mamun, R. W. Sudibyo, and W.-C. Kao, An extension of throughput drop estimation model for three-link concurrent communications under partially overlapping channels and channel bonding in IEEE 802.11n WLAN, Adv. Sci. Technol. Eng. Syst. J., vol. 4, no. 4, pp. 94-105, 2019.
[13] K. I. Munene, N. Funabiki, H. Briantoro, M. M. Rahman, F. Akhter, M. Kuribayashi, and W. -C. Kao, A throughput drop estimation model for concurrent communications under partially overlapping channels without channel bonding and its application to channel assignment in IEEE 802.11n WLAN, IEICE Trans. Inform. Syst., vol. E104-D, no. 5, pp. 585-596, May, 2021.
[14] K. S. Lwin, N. Funabiki, C. Taniguchi, K. K. Zaw, M. S. A. Mamun, M. Kuribayashi, and W. -C. Kao, A minimax approach for access point setup optimization in IEEE 802.11n wireless networks, Int. J. Netw. Comp., vol. 7, no. 2, pp. 187-207, July, 2017.
[15] K. Zhou, X. Jia, Y. Chang, and X. Tang, Partially overlapping channel assignment for WLANs using SINR interference model, Int. J. Commun. Syst, vol. 27, no. 11, pp. 3082-3095, March, 2014.
[16] A. Mishra, E. Rozner, S. Banerjee, and W. Arbaugh, Exploiting partially overlapping channels in wireless networks: turning a peril into an advantage, in Proc. Conf. Inter. Meas., pp. 311-316, 2005.
[17] A. Mishra, V. Shrivastava, S. Banerjee, and W. Arbaugh, Partially overlapped channels not considered harmful, in Proc. IMC, pp. 63-74, 2006.
[18] G. Zhao, Q. Wang, C. Xu, and S. Yu, Analyzing and modeling the interference impact on energy efficiency of WLANs, in Proc. ICC, pp. 1-6, May, 2018.
[19] W. Zhao, H. Nishiyama, Z. Fadlullah, N. Kato, and K. Hamaguchi, DAPA: capacity optimization in wireless networks through a combined design of density of access points and partially overlapped channel allocation, IEEE Trans. Vehi. Tech., vol. 65, no. 5, pp. 3715-3722, May, 2016.
[20] S. Mukherjee, and S. C. Ghosh, Throughput improvement using partially overlapping channels in WLAN with heterogeneous clients, Wired/Wirel. Inter. Commun., pp. 335-347, 2016.
[21] T. Vanhatupa, M. Hännikäinen, and T. D. Hämäläinen, Evaluation of throughput estimation models and algorithms for WLAN frequency planning, Comp. Netw., vol. 51, no. 11, pp. 3110-3124, 2007.
[22] A. Nabil, M. J. Abdel-Rahman, A. B. MacKenzie, and F. Hassan, A stochastic optimization framework for channel bonding in wireless LANs under demand uncertainty, IEEE Trans. Wirel. Comm., vol. 19, no. 11, Nov., pp. 7528-7542, 2020.
[23] B. P. Tewari and S. C. Ghosh, Combined power control and partially overlapping channel assignment for interference mitigation in dense WLAN, in Proc. Int. Conf. Adv. Info. Netw. Appl., pp. 646-653, 2017.
[24] B. P. Tewari and S. C. Ghosh, Efficient AP placement through power control and partially overlapping channel assignment, Wirel. Person. Commu. vol. 110, pp. 223-244, 2020.
[25] A. Kachroo, J. Park , and H. Kim, Channel assignment with transmission power optimization method for high throughput in multi-access point WLAN, in Proc. Wire. Commu. Mob. Comp. Conf., pp. 314-319, 2015.
[26] M. Raval, S. Bhardwaj, A. Aravelli, J. Dofe, and H. Gohel, Smart energy optimization for massive IoT using artificial intelligence, Internet of Things, vol. 13, pp. 100354, 2021.
[27] D. B. Faria, Modeling signal attenuation in IEEE 802.11 wireless LANs, Tech. Report, TRKP06-0118, Stanford Univ., July, 2005.
[28] N. Funabiki, C. Taniguchi, K. S. Lwin, K. K. Zaw, and W- C. Kao, A parameter optimization tool and its application to throughput estimation model for wireless LAN, Proc. Int. Work. Virtual Environ. Netw.-Orient. Appli., pp. 701-710, July, 2017.
[29] I. M. Kwenga, N. Funabiki, M. M. Islam, M. Kuribayashi, R. W. Sudibyo, and W. -C. Kao, A throughput estimation model under two-link concurrent communications with partially overlapping channels and its application to channel assignment

in IEEE 802.11n WLAN, Int. J. Space-Base. Situ. Comp., vol. 8, no. 3, pp. 123-137, 2018.
[30] OriginLab [online], https://www.originlab.com/ (accessed: 15 May 2018 - 10 August 2021).
[31] Y. Su, Y. Wang, Y. Zhang, Y. Liu, and J. Yuan, Partially overlapped channel interference measurement implementation and analysis, Proc. IEEE Conf. Comp. Commun. Work., pp. 760-765, April 2016.
[32] M. Yofune, M. Suto, Y. Amezawa, and S. Sato, Rate-adaptation scheme for multiband wlan system, in Advances in Wireless and Optical Communications (RTUWO), pp. 72-77, 2018.
[33] M. A. Santos, J. Villalón and L. Orozco-Barbosa, Rate adaptation algorithm for 802.11 networks: a dynamic decision approach, 5th Joint IFIP Wireless and Mobile Networking Conference (WMNC), pp. 75-80, 2012.
[34] I. Sammour and G. Chalhoub, Evaluation of rate adaptation algorithms in IEEE 802.11 networks, Electronics, no. 9, pp. 1436, 2020.
[35] Cisco network [online], https://networklessons.com/cisco/ccie-routing-switching-written/tcp-window-size-scaling. (accessed: 2 Feb. 2022).
[36] K. S. Lwin, N. Funabiki, S. K. Debnath, I. M. Kwenga, R. W. Sudibyo and M. Kuribayashi, Enhancements of minimax access-point setup optimisation approach for IEEE 802.11 WLAN, Int. J. Space-Base. Situ. Comp., vol. 9, no. 1, pp. 47-59, 2019.
[37] Iperf - TCP, UDP and SCTP network bandwidth measurement tool, [online], https://iperf.fr/ (accessed: 29 Dec. 2019).
[38] Aterm NEC router [online], https://www.aterm.jp/product/atermstation/trademark.html (accessed: 24 Nov., 2020).
[39] Toshiba dynabook R731/B [online], https://drp.su/en/laptops/toshiba/dynabook-r731-b/wifi?os=windows-10-x64 (accessed: 20 Oct., 2020).
[40] Fujitsu lifebook S761 [online], https://www.cnet.com/products/fujitsu-s761/ (accessed: 20 Oct., 2020).
[41] L. B. Jiang and S. C. Liew, Improving throughput and fairness by reducing exposed and hidden nodes in 802.11 networks, IEEE Trans. Mob. Comp., vol. 7, no. 1, pp. 34-49, Jan. 2008.
[42] H. Briantoro, N. Funabiki, M. M. Rahman, K. I. Munene, and M. Kuribayashi, Joint optimization method of channel assignment and transmission power for concurrently communicating multiple access-points in wireless local-area network, Int. J. Netw. Comp., vol 11, no. 2, pp. 251-266, July 2021.
[43] M. M. Islam, N. Funabiki, M. Kuribayashi, M. Saha, K. I. Munene, R. W. Sudibyo and W.-C. Kao, A proposal of transmission power minimization extension in active access-point configuration algorithm for elastic wireless local-area network system, Int. J. Comp. Soft. Eng. vol. 4, pp. 1-9, 2019
[44] S. K. Debnath, N. Funabiki, K. S. Lwin, M. S. A. Mamun, R. W. Sudibyo, and S. Huda, Raspberry Pi configuration for access-point and its throughput measurements in IEEE802.11n wireless networks, IEICE Tech. Rep., NS2016-137, pp. 101-106, 2016.
[45] Raspberry Pi official website [online], https://www.raspberrypi.com/products/raspberry-pi-3-model-b/ (accessed: 30 Sept., 2020).
[46] TP-Link TL-WN722N [online], https://www.tp-link.com/us/home-networking/usb-adapter/tl-wn722n/ (accessed: 28 Oct., 2019).
[47] M. S. A. Mamun, N. Funabiki, K. S. Lwin, M. E. Islam, and W.-C. Kao, A channel assignment extension of active access-point configuration algorithm for elastic WLAN system and its implementation using Raspberry Pi, Int. J. Netw. Comp., vol. 7, no. 2, pp. 248-270, July, 2017.